Dynamic contrast-enhanced susceptibility-weighted perfusion imaging of intracranial tumors: a study using a 3T MR scanner

Senem Şentürk, Kader Karlı Oğuz, Ayşenur Cila

PURPOSE
To determine whether there are statistically significant differences in cerebral blood volume (CBV) and cerebral blood flow (CBF) of brain tumors of different histopathologic types including primary and secondary benign and malignant lesions. To determine whether these measurements relate to tumor grade.

MATERIALS AND METHODS
Forty-five patients with brain tumors, age 2 to 79 years, underwent dynamic contrast-enhanced susceptibility-weighted echo-planar perfusion magnetic resonance imaging (MRI) using a 3T MR scanner. The lesions were evaluated by measurements of relative cerebral blood volume (rCBV) and relative cerebral blood flow (rCBF). The Mann-Whitney U test was used to compare rCBV and rCBF measurements of tumor groups—13 low-grade and 13 high-grade neuroepithelial (NE) tumors, five metastases, 10 meningiomas, and four others. Peritumoral rCBV and rCBF measurements of high grade NE tumors and metastases were also compared. The relationship between rCBV and rCBF measurements was evaluated by Spearman rank correlation.

RESULTS
Measurements of rCBV and rCBF were statistically significantly higher ($P < 0.05$) in high-grade NE tumors than in low-grade NE tumors. The difference was not statistically significant in comparing high-grade NE tumors with metastases and meningiomas. Peritumoral rCBV of high-grade NE tumors was significantly higher than peritumoral rCBV of metastases ($P < 0.05$). There was a strong correlation between rCBV and rCBF values.

CONCLUSION
CBV and CBF measurements provided by 3T perfusion MRI can help to predict NE tumor grading preoperatively, and differentiate between primary brain tumors and metastases.

Key words: • *brain neoplasms* • *magnetic resonance imaging* • *3 Tesla* • *perfusion weighted imaging*

From the Department of Radiology (S.Ş. ✉ ssenturk@dicle.edu.tr), Dicle University School of Medicine, Diyarbakır, Turkey; and the Department of Radiology (K.K.O., A.C.), Hacettepe University School of Medicine, Ankara, Turkey.

Modern magnetic resonance imaging (MRI) techniques facilitate the acquisition of physiological and biochemical maps, which complement the anatomic information provided by conventional techniques. MR perfusion imaging techniques are becoming important clinical tools in the diagnosis, follow-up, and treatment of patients with brain tumors, cerebrovascular disease, and other brain disorders (1–5).

Although conventional magnetic resonance imaging (cMRI) is a well-established tool for the evaluation of brain tumors, contrast enhancement has limited specificity (6). Precise delineation of tumor margins, and discrimination between tumors and nonneoplastic processes, and between low-grade and high-grade tumors, are all required for preoperative evaluation of space-occupying lesions in the brain.

Astrocytoma is graded according to the following histopathologic criteria: nuclear atypia, mitotic rate, extent of necrosis, and endothelial proliferation (7). Studies of human brain tumors have revealed that increased malignancy is generally associated with increased vascularity. High grade astrocytomas often contain new vessels (neovascularization), irregular vascular networks, and arteriovenous shunts (8, 9).

Since treatment and prognosis depend on the histopathologic type and grade of the tumor, noninvasive preoperative assesment of tumor vascularization can assist in treatment, provide guidance to optimize biopsy yield, and refine prognosis. Previous studies have shown that cerebral blood volume (CBV) measurements provided by perfusion-weighted imaging (PWI) correlate not only with histopathologic measurements, but also with conventional angiographic measurements of tumor vascular density (10–12). These features have facilitated the use of CBV measurements clinically for initial evaluation and follow-up of brain tumors. PWI was found to be useful in guiding stereotactic biopsy, and in delineating exact tumor margins (11, 13). It is also useful in differentiating neoplastic from nonneoplastic processes such as radiation necrosis, tumefactive demyelinating lesions, and inflammatory or infectious lesions (1, 14–17), and in differentiating primary brain tumors from solitary metastases (18–20); as well as in preoperative tumor grading (10–12, 21, 22).

In this study, we sought to determine whether there is a statistically significant difference in the CBV and cerebral blood flow (CBF) of consecutive brain tumors of various histopathologic types—either primary or secondary, benign or malignant—as well as of the peritumoral parenchyma. We also sought to learn whether these measurements are related to tumor grade.

Materials and methods

The study group consisted of 45 consecutive patients (15 females, 30 males) referred to the radiology department with intra- or extra-axial

brain tumors. Patients ranged in age from 2 to 79 years. Except for three patients with postoperative gross residual or recurrent tumors [a residual primitive neuroectodermal tumor (PNET), a residual meningioma, and a recurrent glial tumor of the contralateral hemisphere] all patients were evaluated prior to any medical and surgical treatment. Study approval was obtained from the institutional review board, and written informed consent was obtained from all patients.

Before examination, an 18- or 20-Gauge intravenous catheter was inserted into the antecubital vein in each patient over 7 years of age for administration of contrast. Imaging was performed on a 3T MR scanner (Magnetom Allegra; Siemens Medical Systems, Erlangen, Germany). After cMRI (axial T1W, T2W, and FLAIR; coronal T2W images), dynamic contrast-enhanced T2*W gradient-echo (GRE) echo-planar imaging (EPI) was performed during the first pass of a bolus of gadopentetate dimeglumine (Magnevist; Schering, Berlin, Germany). Finally, postcontrast axial, coronal, and sagittal T1W images were obtained.

PWI was performed by using a fat-suppressed T2*W EPI with the following parameters: repetition time (TR), 1430 ms; echo time (TE), 46 ms; field of view (FOV), 230 x 230 mm; section thickness, 5 mm; section gap, 10 mm; matrix, 128 x 256. The location and size of the tumor, and the scan area of perfusion MRI were determined from T2W MR images. A series of 50 multisection acquisitions with 15 slices was acquired. The first five acquisitions were performed to establish a baseline prior to administration of contrast. On the fifth acquisition, the contrast material (0.1 mmol/kg) was injected with a power injector (Medrad, Pittsburgh, Pennsylvania, USA) at a rate of 5 mL/s in patients over age seven, and a at rate of 1–2 ml/s in those under seven. Finally, a bolus of the same volume of saline was injected with the same rate of administration as the gadolinium-based contrast material in each group.

Study groups

Thirty-nine patients who underwent either volumetric resection or biopsy had histopathologically proven tumors. Six patients were followed for two to four years without surgery.

Their diagnoses were obtained by MRI, and clinical follow-up.

1. High-grade neuroepithelial (NE) tumors (n =13): The pathologic diagnosis was obtained in all patients by either total resection or by biopsy (eight glioblastoma multiforme, two grade 3 glial tumors, one grade 3 oligodendroglioma, and two PNETs).

2. Low-grade NE tumors (n =13): Twelve patients had pathologically proven tumors diagnosed either by resection or by biopsy (seven low-grade astrocytomas, one solid pilocytic astrocytoma, three grade 2 oligodendrogliomas, one DNET [dysembryoblastic neuroectodermal tumor], and one ganglioglioma). The tumor of the remaining patient did not show clinical and radiologic progression during the 4-year follow up. Thus, it was included in low-grade group.

3. Meningiomas (n = 10): The pathologic diagnosis was obtained in nine of the patients (seven grade 1, two grade 2). The remaining patient was diagnosed with clinical and radiologic findings and follow-up.

4. Metastases (n = 5): All patients had pathologically proven primary tumors; however, only two of them underwent surgery for metastases. Four patients had multiple lesions.

5. Miscellaneous (n = 4): One hemangioblastoma and two medulloblastomas diagnosed by pathology were not included in the other tumor groups because of their discrete biologic properties. One patient had a cystic lesion with a mural nodule consistent with a pilocytic astrocytoma. This tumor was not included in low-grade glial tumors because differentiation from hemangioblastoma was not possible. Miscellaneous tumors were not excluded from study groups because the information obtained from these tumors was used not only in morphologic analysis, but also in correlation analysis.

Data processing

Data processing in this study was performed by commercial software on a workstation provided by the vendor (perfusion software, Leonardo work-

station, Siemens, Germany). The CBV map was derived on a pixel-by-pixel basis from the dynamic image sets. A representative number of baseline points were selected, and their average was calculated for each pixel as a baseline measure for signal intensity (S_0). The concentration of the contrast agent (gadopentetate dimeglumine) is proportional to the change in relaxation rate ($\Delta R2^*$), which can be calculated from the signal by using the following equation (23): $\Delta R2^* = [-\ln (S_t/S_0)/TE]$, where St is the pixel signal intensity at time t, S_0 is the precontrast signal intensity, and the TE is the echo time. The CBV map was generated by the integration of the relative concentration ($\Delta R2^*$) of the fist-pass bolus through each voxel on the basis of tracer kinetics principles (24–26). The beginning and end of the first-pass bolus is determined by time-signal activity curve of manually selected referance voxels.

In this study, arterial input function (AIF) was obtained by manually positioning a 20 x 20 pixel region-of-interest (ROI) box on the area covering the M2 portion of middle cerebral artery. AIF was calculated automatically from the manually-selected pixels that contained the earlier and larger relaxation after contrast injection (27). The earlier and larger signal change, consistent with the higher concentration of contrast material in the arteries than in the capillaries of gray matter, was found to be the most suitable AIF (22). To obtain tissue response function, AIF was deconvolved from measured tissue concentration-time curve. Maps of mean transit time (MTT) were obtained by dividing area under the tissue response function by its height (28). CBF was measured by dividing the CBV, obtained from the area below the tissue concentration-time curve, by MTT. With the numeric integration of CBF values, CBF maps were constituted. Examples of CBV and CBF maps are shown in Figs. 1 and 2.

The highest color levels of the solid portion of a tumor, representing a high index of microvascularization, were determined from these semi-automatically obtained CBV and CBF maps. Measurements were then performed by manually positioning a round ROI in the highest color levels (Fig. 3). The size of the ROI was dependent on the size and heterogeneity of the tumor;
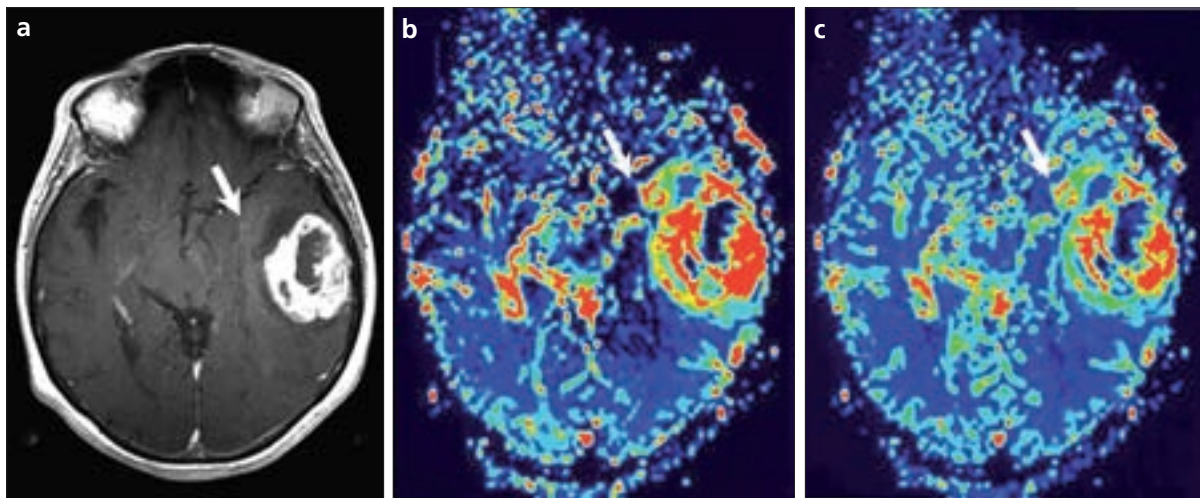
Figure 1. a–c. Left temporal glioblastoma multiforme in a 69-year-old man. Transverse post-contrast T1-weighted MR image **(a)** demonstrates a heterogenously enhancing mass with central necrosis. On relative cerebral blood volume (rCBV) **(b)** and relative cerebral blood flow (rCBF) **(c)** maps, there are high CBV and CBF color values in the solid portion, and very low values in the necrotic portion of the tumor. Note the mismatch area *(white arrows)* between perfusion map **(b, c)** and contrast-enhanced T1-weighted MR image **(a)**.
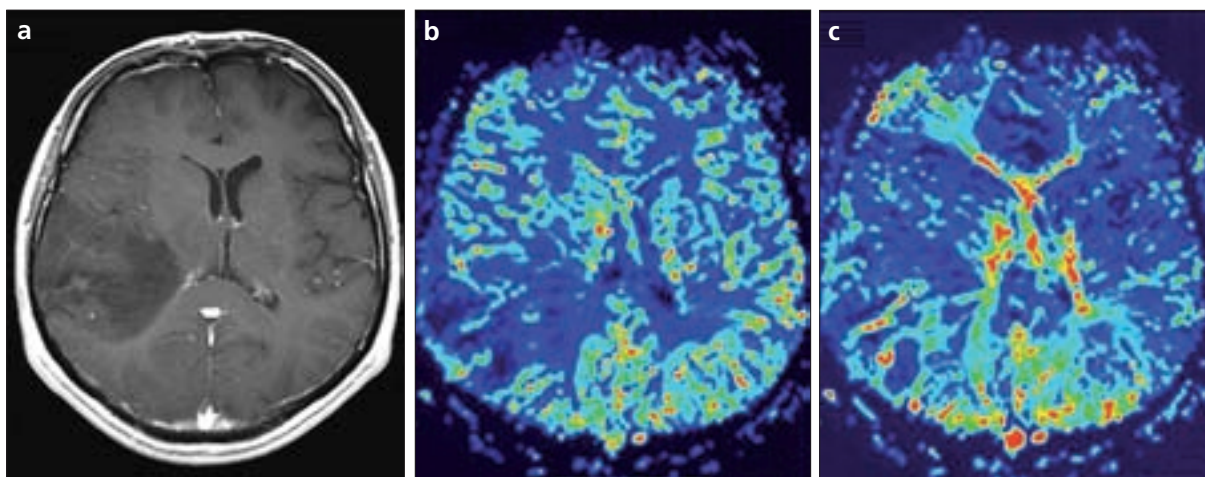
Figure 2. a–c. Right temporal low-grade glial tumor in a 72-year-old man. Transverse post-contrast T1-weighted MR image **(a)** demonstrates a nonenhancing mass. On color relative cerebral blood volume (rCBV) **(b)** and relative cerebral blood flow (rCBF) **(c)** maps, there are correspondingly low CBV and CBF color values.
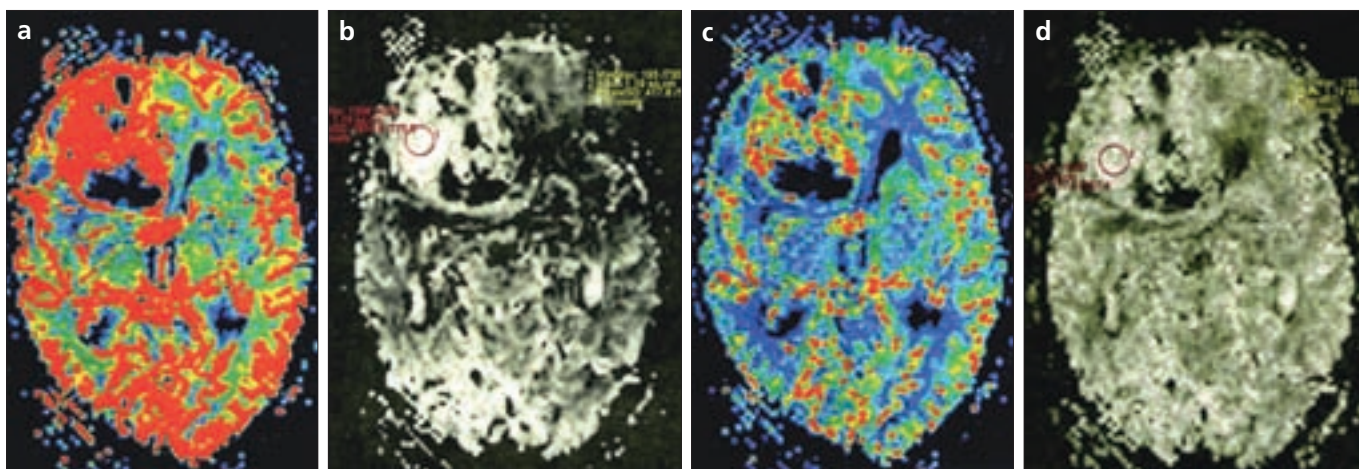
Figure 3. a–d. For relative cerebral blood volume (rCBV) **(a, b)** and relative cerebral blood flow (rCBF) **(c, d)** measurements, highest color levels are determined on color rCBV and rCBF maps **(a, c)**, and region of interests (ROIs) (within high color values of tumor and contralateral white matter) are selected **(b, d)**.

however, each ROI contained at least 18 pixels.

Because CBV and CBF maps provided by dynamic contrast-enhanced T2* PWI yield a relative rather than absolute value of CBV and CBF, comparision between patients was facilitated by reference to an internal standard in this study. Normal white matter of the contralateral hemisphere was used as the internal standard. To calculate relative CBV (rCBV) and relative CBF (rCBF), the ratio of the measurement of tumor ROI to the measurement of white matter ROI was obtained. The highest value of three calculations from the highest color levels of the tumor was taken as the final rCBV and rCBFs because the goal was to determine the most highly perfused portion of the tumor.

Measurements were repeated in peritumoral regions of both high-grade glial tumors and metastases. Peritumoral region was defined as the nonenhancing T2W hyperintense area adjacent to the enhancing portion of the tumor.

The Mann-Whitney U test was used to compare rCBV and rCBF measurements of low- and high-grade NE tumors, high-grade NE tumors and meningiomas, and high-grade NE tumors and metastases. Peritumoral rCBV and rCBF measurements of high-grade NE tumors and metastases were also compared. The relationship between rCBV and rCBF measurements of all 45 tumors was searched by Spearman rank correlation.

Results

There were no side effects related to either the rapid injection of contrast material or to the contrast agents used in the study. Although T2*W GRE EPI technique is affected by susceptibility artifacts, we were able to obtain images of sufficient quality to calculate the rCBV and rCBF of all lesions including posterior fossa tumors.

Of the 45 patients, 39 underwent surgery, while six were diagnosed by clinical and radiologic follow-up up to four years after imaging.

rCBV and rCBF measurements of all tumors are listed in Table 1 with age and gender of patients.

The comparison of cMRI findings with perfusion maps is shown in Table 2. Although contrast-enhanced portions of tumors generally showed high rCBV and rCBF values, a per-

Table 1. Relative cerebral blood volume (rCBV) and relative cerebral blood flow (rCBF) measurements

Patient no.	Age	Gender	Tumor	Tumor grade	rCBV	rCBF
1	42	M	GBM	High	4.73	3.23
2	54	F	GBM	High	9.40	5.91
3	56	M	GBM	High	8.32	2.61
4	69	M	GBM	High	5.63	3.53
5	55	M	GBM	High	13.00	4.75
6	37	M	GBM	High	4.37	3.29
7	62	F	GBM	High	6.47	6.67
8	49	M	GBM	High	5.62	7.01
9	64	M	Grade 3 glial tumor	High	6.02	6.41
10	17	M	Grade 3 glial tumor	High	3.10	3.37
11	46	M	Oligodendroglioma, grade 3	High	3.57	3.76
12	9	F	PNET	High	5.30	8.66
13	10	M	PNET	High	12.73	5.16
14	17	M	DNET	Low	3.69	1.65
15	9	M	Ganglioglioma	Low	1.87	1.24
16	4	M	Pilocytic astrocytoma	Low	3.16	1.76
17	49	F	Low grade glial tumor	Low	1.97	1.28
18	2	M	Low grade glial tumor	Low	2.30	3.34
19	65	M	Low grade glial tumor	Low	3.32	3.18
20	49	F	Low grade glial tumor	Low	1.67	1.74
21	41	M	Low grade glial tumor	Low	4.22	0.95
22	62	M	Low grade glial tumor	Low	3.38	3.22
23	72	M	Low grade glial tumor[a]	Low	0.84	1.01
24	41	M	Oligodendroglioma, grade 2	Low	3.24	3.90
25	43	M	Oligodendroglioma, grade 2	Low	2.07	1.98
26	45	M	Oligodendroglioma, grade 2	Low	1.16	1.36
27	57	M	Metastasis, lung[a]		17.46	6.98
28	69	M	Metastasis, lung[a]		12.73	3.79
29	43	F	Metastasis, breast[a]		6.09	4.30
30	53	M	Metastasis, lung		6.38	4.76
31	57	M	Metastasis, lung		8.11	2.25
32	69	M	Meningioma		27.71	11.04
33	40	M	Meningioma		7.27	4.46
34	54	F	Meningioma[a]		13.03	8.47
35	79	F	Atypical meningioma, grade 2		19.47	7.39
36	77	F	Meningioma, grade 2		18.67	7.78
37	55	F	Meningioma		2.49	3.52
38	59	F	Meningioma		5.73	3.74
39	55	F	Meningioma, grade 1		7.35	5.78
40	43	F	Meningioma, grade 1		4.13	4.19
41	51	F	Meningioma, grade 1		7.27	9.09
42	29	M	Hemangioblastoma		3.68	5.87
43	6	F	Medulloblastoma		1.67	1.06
44	5	M	Medulloblastoma		3.59	1.58
45	18	M	Pilocytic astrocytoma[a]		12.8	6.17

M, male; F, female; GBM, glioblastoma multiforme; PNET, primitive neuroectodermal tumor; DNET, dysembryoblastic neuroectodermal tumor; rCBV, relative cerebral blood volume; rCBF, relative cerebral blood flow
[a] Clinical and radiologic diagnosis of patients who did not undergo surgical resection or biopsy

Table 2. Conventional contrast-enhanced MRI and colored cerebral blood volume (CBV) maps

Patient no.	Tumor	Location	Conventional MRI findings	CBV maps
1	GBM	Right parietal	Heterogenous intense enhancement and necrosis	Heterogenous high CBV in solid portions, very low CBV in necrotic areas
2	GBM	Right frontal	Heterogenous intense enhancement and necrosis	Heterogenous high CBV in solid portions, very low CBV in necrotic areas
3	GBM	Left frontotemporal	Peripheral intense enhancement and central necrosis	Peripheral high CBV, central very low CBV
4	GBM[a]	Left frontotemporal	Peripheral intense enhancement and central necrosis	Peripheral high CBV, central very low CBV
5	GBM	Right occipital	Peripheral intense enhancement and central necrosis	Peripheral high CBV, central very low CBV
6	GBM[a]	Left parietal	Mild-moderate enhancement and nonenhancing components	Heterogenous moderate CBV
7	GBM	Left temporal	Heterogenous intense enhancement and necrosis	Heterogenous high CBV in solid portions, very low CBV in necrotic areas
8	GBM[a]	Right parietal	Heterogenous intense enhancement and necrosis	Heterogenous high CBV in solid portions, very low CBV in necrotic areas
9	Grade 3 glial tumor	Left frontal	Heterogenous mass, nodular enhancement	Low CBV mass with high CBV in the nodules
10	Grade 3 glial tumor	Third ventricle	Peripheral intense enhancement and central necrosis	Peripheral high CBV, central very low CBV
11	Oligodendroglioma	Left frontal	Homogenous nonenhancing mass	Heterogenous low CBV
12	PNET	Cerebellar vermis	Heterogenous enhancement and cystic-necrotic components	Heterogenous high CBV in solid portions, very low CBV in cystic component
13	PNET[a]	Left frontotemporal	Heterogenous enhancement and cystic-necrotic components	Heterogenous high CBV in solid portions, very low CBV in necrotic areas
14	DNET	Right cerebellar	Heterogenous enhancement and cystic components	Heterogenous low CBV in solid portions, very low CBV in cystic components
15	Ganglioglioma	Right temporo-occipital	Cystic lesion with enhancing mural nodule	High CBV mural nodule in very low CBV of cyst
16	Pilocytic astrocytoma	Left frontotemporal	Heterogenous mild-moderate enhancement	Moderate CBV
17	Low grade glial tumor	Right frontal	Homogenous nonenhancing mass	Homogenous low CBV
18	Low grade glial tumor	Left temporal	Heterogenous mild-moderate enhancement	Homogenous low CBV
19	Low grade glial tumor	Left frontotemporal	Homogenous nonenhancing mass	Homogenous low CBV
20	Low grade glial tumor	Left frontal	Nonenhancing mass with small cystic component	Low CBV in solid portions, very low CBV in cystic component
21	Low grade glial tumor	Right temporoparietal	Nonenhancing mass with multiple small cysts	Low CBV in solid portions, very low CBV in cystic components
22	Low grade glial tuomr	Right perisylvian	Heterogenous mild enhancement	Homogenous low CBV
23	Low grade glial tumor[b]	Right frontotemporal	Homogenous nonenhancing mass	Homogenous low CBV
24	Oligodendroglioma	Left frontal	Heterogenous mild enhancement and calcification	Homogenous low CBV
25	Oligodendroglioma	Right occipital	Homogenous nonenhancing mass	Homogenous low CBV
26	Oligodendroglioma	Right temporal	Homogenous nonenhancing mass	Homogenous low CBV
27	Metastasis, lung[b]	Left frontal	Heterogenous intense nodular enhancement	Heterogenous high CBV, very low CBV at peripheral edema

GBM, glioblastoma multiforme; PNET, primitive neuroectodermal tumor; DNET, dysembrioblastic neuroectodermal tumor; CBV, cerebral blood volume
[a] Tumors that showed a mismatch between the area enhancing most intensively on post-contrast T1-weighted MR images and the area of the highest color value on the cerebral blood volume (CBV) and cerebral blood flow (CBF) maps
[b] Clinical and radiologic diagnosis of patients who did not undergo surgery or biopsy

Table 2 (continued). Conventional contrast-enhanced MRI and colored cerebral blood volume (CBV) maps

Patient no.	Tumor	Location	Conventional MRI findings	CBV maps
28	Metastasis, lung[b]	Right frontal	Heterogenous intense nodular enhancement	Heterogenous high CBV, very low CBV at peripheral edema
29	Metastasis, breast[b]	Left temporal	Heterogenous intense nodular enhancement	Heterogenous high CBV, very low CBV at peripheral edema
30	Metastasis, lung	Right parietooccipital	Peripheral dense enhancement and central necrosis	Peripheral high CBV, low CBV at the center and peripheral edema
31	Metastasis, lung	Left temporal	Heterogenous intense nodular enhancement	Heterogenous high CBV, very low CBV in peripheral edema
32	Meningioma	Left parietooccipital convexity	Homogenous intense enhancement	Homogenous high CBV
33	Meningioma	Right frontal base	Homogenous intense enhancement	Homogenous high CBV
34	Meningioma[b]	Left frontal parafalcian	Homogenous intense enhancement and calcification	Homogenous high CBV
35	Meningioma, grade 2	Left infratentorial	Homogenous intense enhancement	Homogenous high CBV
36	Meningioma, grade 2	Right frontal convexity	Homogenous intense enhancement	Homogenous high CBV
37	Meningioma	Posterior fossa, sigmoid dura	Homogenous intense enhancement	Homogenous high CBV
38	Meningioma	Right parafalcian	Heterogenous intense enhancement	Heterogenous high CBV
39	Meningioma	Left sphenoid wing	Homogenous intense enhancement	Homogenous high CBV
40	Meningioma	Left anterior temporal	Homogenous intense enhancement and punctate calcifications	Homogenous high CBV
41	Meningioma	Olfactory groove	Homogenous intense enhancement	Homogenous high CBV
42	Hemangioblastoma	Brain stem and thalamus	Cystic lesion with enhancing mural nodule	High CBV mural nodule in a cyst with very low CBV
43	Medulloblastoma	Cerebellar vermis	Heterogenous enhancement and cystic components	Heterogenous low CBV with very low CBV in cystic components
44	Medulloblastoma	Fourth ventricle	Heterogenous mild enhancement	Heterogenous moderate CBV
45	Pilocytic astrocytoma[b]	Left cerebellar	Cystic lesion with enhancing mural nodule	High CBV mural nodule in a cyst with very low CBV

GBM, glioblastoma multiforme; PNET, primitive neuroectodermal tumor; DNET, dysembrioblastic neuroectodermal tumor; CBV, cerebral blood volume
[a] Tumors that showed a mismatch between the area enhancing most intensively on post-contrast T1-weighted MR images and the area of the highest color value on the cerebral blood volume (CBV) and cerebral blood flow (CBF) maps
[b] Clinical and radiologic diagnosis of patients who did not undergo surgery or biopsy

fusion abnormality was also found in nonenhancing portions of tumors (Fig. 1, Fig. 4). Increased perfusion values were determined in non-enhancing portions of two high-grade NE tumors.

The distribution of rCBV and rCBF values of tumor groups is plotted in Figs. 5 and 6.

Mean rCBV and rCBF values of all tumor groups (high-grade NE tumors, low-grade NE tumors, metastases, and meningiomas) were calculated for each group.

rCBV and rCBF observations are summarized in Tables 3 and 4, respectively. Peritumoral rCBV measurements of high-grade NE tumors and metastases are listed in Table 5.

The difference between rCBV values of low-grade NE tumors (mean, 2.53 ± 1.05) and high-grade NE tumors (mean, 6.79 ± 3.17) was statistically significant ($P < 0.05$). The rCBF values of low-grade NE tumors (mean, 2.05 ± 1.05) were also significantly lower ($P < 0.05$) than rCBF values of high-grade NE tumors (mean, 4.93 ± 1.91).

When high-grade NE tumors were compared with meningiomas, the rCBV and rCBF values of high-grade NE tumors (mean rCBV, 6.79 ± 3.17; rCBF, 4.93 ± 1.91) were not significantly different from those of meningiomas (mean rCBV, 9.37 ± 1.05; rCBF, 6.55 ± 2.62) ($P > 0.05$).

rCBV and rCBF values of high-grade NE tumors (mean rCBV, 6.79 ± 3.17;

rCBF, 4.93 ± 1.91) and metastases (mean rCBV, 8.95 ± 2.65; rCBF, 4.42 ± 1.72) did not differ significantly ($P > 0.05$); however, peritumoral rCBV values of high-grade NE tumors (mean rCBV, 1.52 ± 1.11) were significantly higher than rCBV values of metastases (mean rCBV, 0.53 ± 0.25) ($P < 0.05$) (Table 5).

A strong correlation between rCBV and rCBF values of all tumors has been determined with the high Spearman's rank correlation coefficient of 0.748 ($P < 0.05$) (Fig. 7).

When morphologic properties of tumors were reviewed, variable rCBV (ranging from 1.87 to 12.8) and rCBF values (ranging from 1.24 to 6.17) were found in cystic tumors with a mural
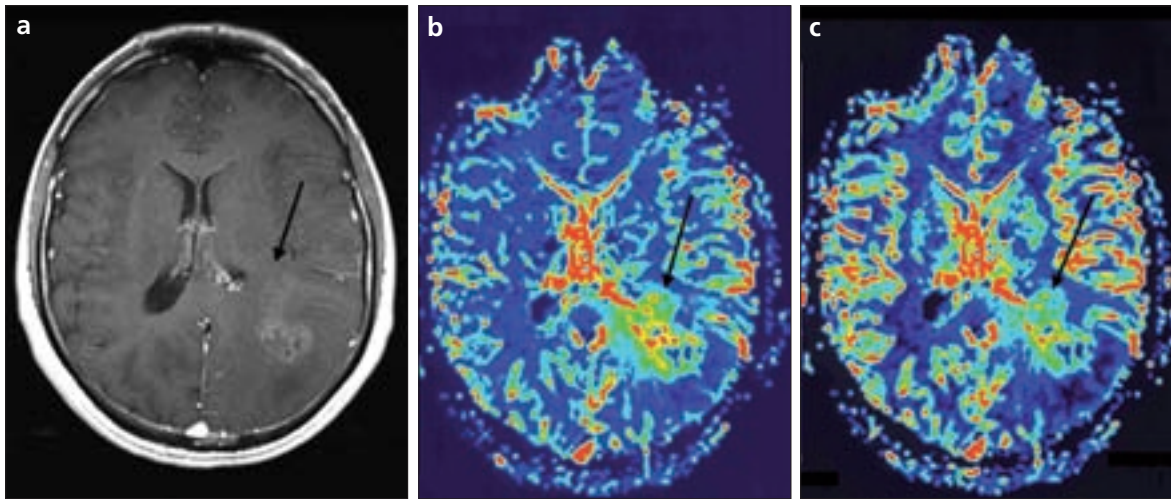
Figure 4. a–c. Left parietooccipital high-grade glial tumor in a 37-year-old man. Transverse post-contrast T1-weighted MR image **(a)** demonstrates a mildly–moderately enhancing mass with nonenhancing portions *(arrow)*. On color relative cerebral blood volume (rCBV) **(b)** and relative cerebral blood flow (rCBF) **(c)** maps, there are moderate–high CBV and CBF color values, respectively *(arrows)*. Note mismatch between perfusion maps **(b, c)** and contrast-enhanced T1-weighted MR image **(a)**.
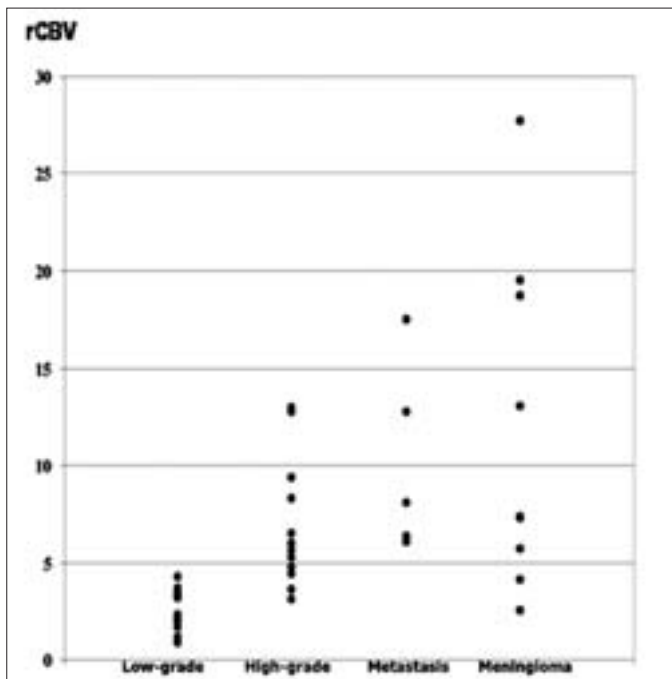
Figure 5. Distribution of relative cerebral blood volume (rCBV) (maximum tumor CBV/contralateral white matter CBV values for each tumor group).
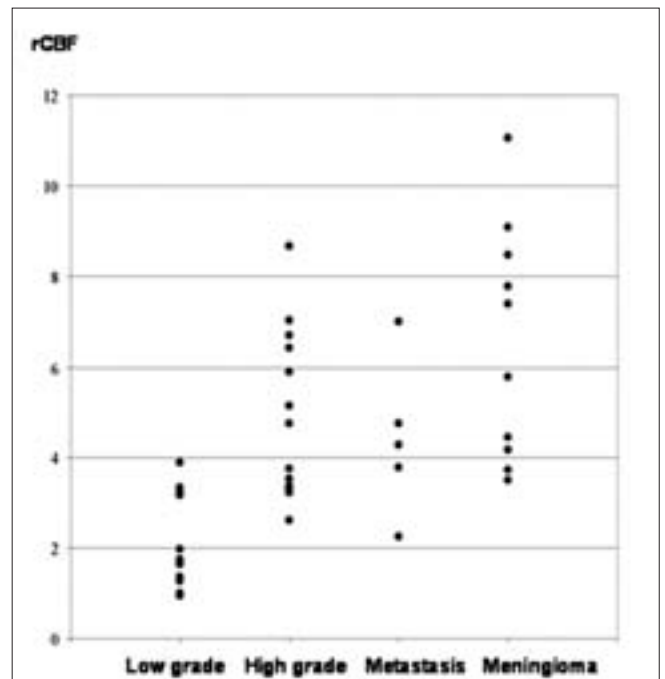
Figure 6. Distribution of relative cerebral blood flow (rCBF) (maximum tumor CBF/ contralateral white matter CBF values for each tumor group).

nodule. These tumors include one gangliocytoma, one hemangioblastoma, one pilocytic astrocytoma, and one tumor without pathologic diagnosis but for which the age of patient and radiologic findings were suggestive of pilocytic astrocytoma. All necrotic tumors were either high-grade NE tumors or metastases. The rCBV values of both high-grade NE tumors and metastases (ranging from 4.73 to 13.0) were higher than those of low-grade NE tumors.

Finally, despite their high grade, one of two posterior fossa medulloblastomas showed relatively low rCBV and rCBF values (rCBV, 1.67; rCBF, 1.06). The other case had slightly to moderately increased rCBV and rCBF values (rCBV, 3.59; rCBF, 1.58).

Discussion

Research on human brain tumors consistently demonstrates that hypervascularity is associated with tumor malignancy. Studies on astrocytomas, the most common primary brain tumors, has shown that neovascularity, irregular vascular networks, and arteriovenous shunts are common in high-grade tumors (8, 9). Therefore, preoperative assessment of tumor vascularization of astrocytomas can help predict malignancy and proliferative potential, and can guide sterotactic biopsy as well as treatment planning (29, 30).
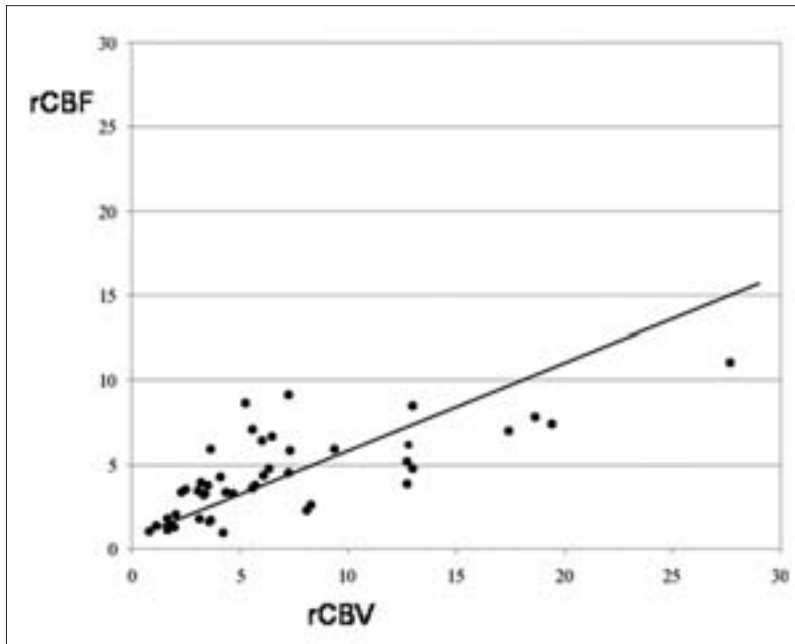
Figure 7. Scatterplot shows high correlation between relative cerebral blood volume (rCBV) and relative cerebral blood flow (rCBF) ratios. Line represents linear regression between rCBV and rCBF ratios. Spearman's correlation coefficient, 0.748 ($P < 0.05$).

Table 3. Relative cerebral blood volume (rCBV) measurements

| Tumor | No. of patients | rCBV ratios | | |
		Range	Mean	Standard deviation
Low-grade NE tumor	13	0.84–4.22	2.53	1.05
High-grade NE tumor	13	3.10–13.00	6.79	3.17
Metastasis	5	6.09–17.46	8.95	2.65
Meningioma	10	2.49–27.71	9.37	1.05

rCBV, relative cerebral blood volume; NE, neuroepithelial

Table 4. Relative cerebral blood flow (rCBF) measurements

| Tumor | No. of patients | rCBF ratios | | |
		Range	Mean	Standard deviation
Low-grade NE tumor	13	0.95–3.90	2.05	1.05
High-grade NE tumor	13	2.61–8.66	4.93	1.91
Metastasis	5	2.25–6.98	4.42	1.72
Meningioma	10	3.52–11.04	6.55	2.62

rCBF, relative cerebral blood flow; NE, neuroepithelial

Table 5. Peritumoral relative cerebral blood volume (rCBV) measurements

| Tumor | No. of patients | rCBV ratios | | |
		Range	Mean	Standard deviation
High-grade NE tumor	13	0.65–4.32	1.52	1.11
Metastasis	5	0.18–0.88	0.53	0.25

rCBV, relative cerebral blood volume; NE, neuroepithelial

Conventional angiographic techniques had been used for years to evaluate tumor vascularity. Nevertheless, since they are invasive and insufficient for assessment of microvascularity, they are not appropriate for evaluation of tumors. With the introduction of ultrafast MRI techniques such as EPI, the microvascularity of brain tumors has been evaluated by PWI. CBV maps provided by perfusion MRI have been shown to be informative for tissue microvascularization. They not only provide qualitative discrimination of capillary neovascularization, but also enable relative quantitative measurements (23, 31, 32). Aronen et al. showed that rCBV values obtained by spin-echo EPI technique correlated well with the histopathologic vascularity grade of glial tumors (10). They also demonstrated that none of the cMRI findings including tumor enhancement, edema, heterogeneity, necrosis, cysts, hemorrhage, mass effect, and ill-defined tumor margins was solely associated with tumor grade (10).

In addition to larger neovascular structures such as feeding arteries and drainage veins, there are larger capillaries in malignant tumors. The GRE EPI technique produces hemodynamic maps by representing the effects of total blood volume through the capillaries, and weighs all vessels approximately equally (33). Sugahara et al. and Donahue et al. showed that rCBV values provided by GRE EPI technique correlated well with the histopathologic and angiographic vascularity grade of tumors (12, 34). We preferred gradient-echo imaging to spin-echo imaging in this study.

Although a statistically significant difference was found between rCBV and rCBF values of low- and high-grade glial tumors, there was no such statistically significant difference between grade 3 and grade 4 tumors (10–12, 35). In this study, regardless of origin, all NE tumors are included in the study group. They are divided into two groups, low- and high-grade NE tumors. Although the significance of microvascularization is not clear in NE tumors other than astrocytomas, in WHO classsification, all NE tumors are graded according to several criteria, including microvascularization (36). Because the difference between rCBV and rCBF values of low- and high-grade NE tumors was statistically

significant, this study suggests that microvascularization also can be important in NE tumors other than astrocytomas.

Of the 12 tumors showing a moderate to strong degree of enhancement on contrast-enhanced T1W MRI, four (33%) displayed a mismatch between the area enhancing most intensely on post-contrast T1W MR images, and the area of the highest color value on the CBV and CBF maps. In two of these mismatched cases, the area with strongest enhancement on post-contrast T1W MR images was larger than the highest color value area on the perfusion maps. This might suggest that the area of vascular hyperplasia is less than the most strongly enhancing area on contrast-enhanced T1W MR examination and might be explained by the fact that contrast enhancement occurs as a result of alteration of the blood-brain barrier with or without concomitant vascular hyperplasia (6). Increased perfusion was determined in non-enhancing portions of the other two remaining tumors on CBV and CBF maps.

The mean rCBV and rCBF values obtained in studies of high- and low-grade glial tumors with 1.5T MR scanners are compatible with our findings (10–12, 22, 35, 37). The mean rCBV and rCBF values of low-grade tumors in this study are a little higher than those in previous studies. Given that rCBV values of oligodendrogliomas are higher than those of low-grade astrocytomas, one may attribute the slightly higher values in our study to the inclusion of non-astrocytomas such as oligodendrogliomas (38, 39).

In a study by Law et al. there was no statistically significant difference between rCBV measurements of PNETs in adults and high-grade glial tumors whereas the rCBV of PNETs was significantly higher than that of low-grade glial tumors (40). The CBV values of the two pediatric patients with PNET also are high (5.30 and 12.73) in this study. The rCBV measurements of anaplastic oligodendrogliomas showed significantly higher rCBV values than low-grade oligodendrogliomas in a study performed by Spampinato et al. (41). Previously published studies and our study demonstrate that PWI plays a role in determining the degree of microvascularization in some other NE tumors, such as oligodendrogliomas, in addition to astrocytomas.

Despite their aggressive behavior and histopathologic grade, one of two posterior fossa medulloblastomas showed low rCBV and rCBF values (rCBV, 1.67; rCBF, 1.06). The other case had low to moderate rCBV and rCBF values (rCBV, 3.59; rCBF, 1.58). To our knowledge, perfusion MRI findings of medulloblastomas have not been reported before.

In this study, we found no statistically significant difference in either rCBV or rCBF when high-grade NE tumors were compared with metastases; however, peritumoral rCBV measurements of high-grade NE tumors were found to be significantly higher than those of metastases. This finding is in agreement with findings of other studies, also performed on 3T MR systems, by Law et al. and Chiang et al. (18, 19). Therefore, this finding suggests that high T2 signal intensity around the primary tumor may represent cellular infiltration, while it shows fluid accumulation due to changes in capillary permeability in metastasis (42). Thus, we believe that PWI could be used in clinical application to distinguish primary tumors from metastases.

PWI was also used in evaluation of meningiomas, e.g. for determination of pre- and post-embolization vascularization (43, 44). Despite the wide range of rCBV values of meningiomas in our study (2.49–27.41)—probably due to leakage, in the absence of a blood-brain barrier—there was no statistically significant difference between rCBV values of high-grade NE tumors and those of meningiomas.

Meningiomas are extraaxial hypervascular tumors that have dual arterial supply from branches of the external carotid artery and internal carotid artery. In the absence of a blood-brain barrier, permeability of their feeding arteries is high. It is not surprising that although the difference was not stastically significant, mean rCBV and rCBF values of meningiomas were the highest of all tumor groups.

Our study group includes heterogenous histopathologic types of tumors. The most important limitations of this study are the heterogenous nature of the study group, and the absence of histopathologic diagnosis and exact grade of tumors in six patients. Although the study includes a small number of tumors other than astrocytomas, the numbers of low- and high-grade tumors are equal.

High Tesla MR systems, which provide higher resolution and faster imaging, are well-suited for PWI of brain tumors; however, there are few previously published studies of brain tumors with high Tesla MR scanners. Additional studies should include more study subjects, and detailed histopathologic correlation with imaging of NE tumors.

Dynamic contrast-enhanced PWI provides important physiological information that cannot be obtained by cMRI. When compared with other imaging techniques such as positron emission tomography (PET) and single photon emission computed tomography (SPECT), dynamic contrast-enhanced PWI is a rapid and less expensive high-resolution imaging modality with greater availability. It may become the preferred modality in preoperative diagnosis and grading of brain tumors, as well as in follow-up after treatment.

References

1. Petrella JR, Provenzale JM. MR perfusion imaging of the brain: techniques and applications. AJR Am J Roentgenol 2000; 175:207–219.
2. Cha S, Knopp EA, Johnson G, Wetzel SG, Litt AW, Zagzag D. Intracranial mass lesions: dynamic contrast-enhanced susceptibility-weighted echo-planar perfusion MR imaging. Radiology 2002; 223:11–29.
3. Keston P, Murray AD, Jackson A. Cerebral perfusion imaging using contrast-enhanced MRI. Clin Radiol 2003; 58:505–513.
4. Law M, Oh S, Babb JS, et al. Low grade gliomas: dynamic susceptibility-weighted contrast-enhanced perfusion MR imaging-prediction of patient clinical response. Radiology 2006; 238:658–667.
5. Provenzale JM, Mukundan S, Barboriak DP. Diffusion-weighted and perfusion MR imaging for brain tumor characterization and assessment of treatment response. Radiology 2006; 239:632–649.
6. Brant-Zawadski M. Pitfalls of contrast enhanced imaging in the nervous system. Magn Reson Med 1991; 22:243–248.
7. Daumas-Duport K, Sheithauer B, O'Fallon J, Kelly P. Grading of astrocytomas: a simple and reproducible method. Cancer 1988; 62:2152–2165.
8. Folkman J. Seminars in medicine of the Beth Israel Hospital, Boston: clinical applications of research on angiogenesis. N Engl J Med 1995; 333:1757–1763.
9. Plate KH, Breier G, Weich HA, Risau W. Vascular endothelial growth factor is a potential tumour angiogenesis factor in human gliomas in vivo. Nature 1992; 359:845–848.
10. Aronen HJ, Gazit EI, Louis DN, et al. Cerebral blood volume maps of gliomas: comparison with tumor grade and histologic findings. Radiology 1994; 191:41–51.

11. Knopp EA, Cha S, Johnson G, et al. Glial neoplasms: dynamic contrast enhanced T2* weighted MR imaging. Neuroradiol 1999; 211:791–798.

12. Sugahara T, Korogi Y, Kochi M, et al. Correlation of MR imaging-determined cerebral blood volume maps with histologic and angiographic determination of vascularity of gliomas. AJR Am J Roentgenol 1998; 171:1479–1486.

13. Wong JC, Provenzale JM, Petrella JR. Perfusion MR imaging of brain neoplasms. AJR Am J Roentgenol 2000; 174:1147–1157.

14. Sugahara T, Korogi Y, Tomiguchi S, et al. Posttherapeutic intraaxial brain tumor: the value of perfusion sensitive contrast-enhanced MR imaging for differentiating tumor recurrence from non-neoplastic contrast-enhancing tissue. AJNR Am J Neuroradiol 2000; 21:901–909.

15. Cha S, Pierce S, Knopp EA, et al. Dynamic contrast-enhance T2*-weighted MR imaging of tumefactive demyelinating lesions. AJNR Am J Neıroradiol 2001; 22:1109–1116.

16. Ernst TM, Chang L, Witt MD, et al. Cerebral toxoplasmosis and lymphoma in AIDS: perfusion MR imaging experience in 13 patients. Radiology 1998; 208:663–669.

17. Erdogan C, Hakyemez B, Yildirim N, Parlak M. Brain abscess and cystic brain tumor: discrimination with dynamic susceptibility contrast perfusion-weighted MRI. J Comput Assist Tomogr 2005; 29:663–667.

18. Law M, Cha S, Knopp EA, Johnson G, Arnett J, Litt AW. High-grade gliomas and solitary metastasis: differentiation by using perfusion and proton spectroscopic MR imaging. Neuroradiology 2002; 222:715–721.

19. Chiang CI, Kuo YT, Lu CY, et al. Distinction between high-grade gliomas and solitary metastasis using peritumoral 3-T magnetic resonance spectroscopy, diffusion, and perfusion imagings. Neuroradiol 2004; 46:619–627.

20. Bulakbasi N, Kocaoglu M, Farzaliyev A, Tayfun C, Ucoz T. Somuncu I. Assessment of diagnostic accuracy of perfusion MR imaging in primary and metastatic solitary brain tumors. AJNR Am J Neıroradiol 2005; 26:2187–2199.

21. Wetzel SG, Cha S, Law M, et al. Preoperative assessment of intracranial tumors with perfusion MR and a volumetric interpolated examination: a comparative study with DSA. AJNR Am J Neroradiol 2002; 23:1767–1774.

22. Shin JH, Lee HK, Kwun BD, et al. Using relative cerebral blood flow and volume to evaluate the histopatologic grade of cerebral gliomas: preliminary results. AJR Am J Roentgenol 2002; 179:783–789.

23. Rosen BR, Belliveau JE, Vevea JM, Brady TJ. Perfusion imaging with NMR contrast agents. Magn Reson Med 1990; 14:249–265.

24. Villringer A, Rosen BR, Belliveau JW, et al. Dynamic imaging with lantanide chelates in normal brain: contrast due to magnetic susceptibility effects. Magn Reson Med 1988; 78:41–55.

25. Rosen BR, Belliveau JW, Chien D. Perfusion imaging nuclear magnetic resonance. Magn Reson Q 1989; 5:263–281.

26. Axel L. Cerebral blood flow determination by rapid-sequence computed tomography: theoretical analysis. Radiology 1980; 137:679–686.

27. Ostergaard L, Sorenson AG, Kwong KK, Weisskoff RM, Gyldensted C, Rosen BR. High resolution measurement of cerebral blood flow using intravascular tracer bolus passages. II. Experimental comparison and preliminary results. Magn Reson Med 1996; 36:726–736.

28. Weisskoff RW, Chesler D, Boxerman JL, Rosen BR. Pitfalls in MR measurement of tissue blood flow with intravascular tracers: which mean transit time? Magn Reson Med 1992; 29:553–559.

29. Leon PS, Folkerth RD, Black PM. Microvessel density is a prognostic indicator for patients with astroglial brain tumors. Cancer 1996; 77:362–372.

30. Glantz MJ, Burger PC, Herdon JE II, et al. Influence of type of surgery on the histologic diagnosis in patients with anaplastic gliomas. Neurology 1991; 41:1741–1744.

31. Belliveau JW, Rosen BR, Kantor HL, et al. Functional cerebral imaging by susceptibility contrast NMR. Magn Reson Med 1990; 14:538–546.

32. Rosen BR, Belliveau JW, Aronen HJ et al. Susceptibility contrast MR imaging of cerebral blood volume: human experience. Magn Reson Med 1991; 22:293–299.

33. Boxerman JL. Hamberg LM. Rosen BR, Weisskoff RM. MR contrast due to intravascular magnetic susceptibility perturbations. Magn Reson Med 1996; 34:555–566.

34. Donahue KM, Krouwer HG, Rand SD, et al. Utility of simultaneously acquired gradient-echo and spin-echo cerebral blood volume and morphology maps in brain tumor patients. Magn Reson Med 2000; 43:845–853.

35. Hakyemez B, Erdogan C, Ercan I, Ergin N, Uysal S, Atahan S. High-grade and low-grade gliomas: differentiation by perfusion MR imaging. Clin Radiol 2005; 60:493–502.

36. Andrew HAH, Laws ER Jr. Brain tumors, an encyclopedic approach. 2nd ed. New York, NY: Churchill Livingstone 2001; 29–45.

37. Law M, Yang S, Wang H, et al. Glioma grading: sensitivity, specificity, and predictive values of perfusion MR imaging and proton MR spectroscopic imaging compared with conventional MR imaging. AJNR Am J Neuroradiol 2003; 24:1989–1998.

38. Lev MH, Ozsunar Y, Henson JW, et al. Glial tumor grading and outcome prediction using dynamic spin-echo MR susceptibility mapping compared with conventional contrast-enhanced MR: confounding effect of elevated rCBV of oligodendrogliomas. AJNR Am J Neuroradiol 2004; 25:214–221.

39. Cha S, Tihan T, Crawford F, et al. Differentiation of low-grade oligodendrogliomas from low-grade astrocytomas by using quantitative blood-volume measurements derived from dynamic susceptibility contrast-enhanced MR imaging. AJNR Am J Neuroradiol 2005; 26:266–273.

40. Law M, Kazmi K, Wetzal S, et al. Dynamic contrast-enhanced perfusion and conventional MR imaging findings for adult patients with cerebral primitive neuroectodermal tumor. AJNR Am J Neuroradiol 2004; 25:997–1005.

41. Spampinato MV, Smith JK, Kwock L, et al. Cerebral blood volume measurements and proton MR spectroscopy in grading oligodendroglial tumors. AJR Am J Roentgenol 2007; 188:204–212.

42. Strugar J, Rothbart D, Harrington W, Criscuolo GR. Vascular permeability factor in brain metastases: correlation with vasogenic brain edema and tumor angiogenesis. J Neurosurg 1994; 81:560–566.

43. Bruening R, Wu RH, Yousry TA, et al. Regional relative blood volume MR maps of meningiomas before and after partial embolization. J Comput Assist Tomogr 1998; 22:104–110.

44. Principi M, Italiani M, Guiducci A, et al. Perfusion MRI in the evaluation of the relationship between tumour growth, necrosis and angiogenesis in glioblastomas and grade 1 meningiomas. Neuroradiol 2003; 45:205–211.